Particle Accelerators, Vol. 62, pp. [537–554]/17–34
Reprints available directly from the publisher
Photocopying permitted by license only

PROTON LINAC ACTIVITIES IN JAERI

NOBUO OUCHI[a,*], JOICHI KUSANO[a], NOBUO AKAOKA[a], SUEHIRO TAKEUCHI[a], BENJAMIN FECHNER[a], KAZUO HASEGAWA[a], MOTOHARU MIZUMOTO[a], HITOSHI INOUE[b], EIJI KAKO[b], SHUICHI NOGUCHI[b], MASAAKI ONO[b], KENJI SAITO[b], KEN MUKUGI[c] and YOICHIRO HONDA[d]

[a]*Japan Atomic Energy Research Institute, Tokai-mura, Naka-gun, 319-11 Ibaraki-ken, Japan;* [b]*KEK: High Energy Accelerator Research Organization, Oho, Tsukuba-shi, 305 Ibaraki-ken, Japan;* [c]*Mitsubishi Electric Corporation, Wadasaki-cho, Hyogo-ku, Kobe-shi, 652 Hyogo-ken, Japan;* [d]*Mitsubishi Heavy Industries, Ltd., Oye-cho, Minato-ku, Nagoya-shi, 455 Aichi-ken, Japan*

(Received in final form 15 January 1998)

Design and development work on the high intensity superconducting proton linac for the Neutron Science Project (NSP) has been proceeding in JAERI. This paper describes the overview of the project and the present status of the conceptual design of the linac and cavity design work.

Keywords: Superconductivity; Radiofrequency; Cavities; Proton linac

1. INTRODUCTION

Japan Atomic Energy Research Institute (JAERI) has been proposing the Neutron Science Project (NSP) for the purpose of investigations in the fields of nuclear transmutation technology and advanced basic science by using the next generation spallation neutron source driven by an intense proton linac.[1] The linac is required to provide the proton

* Corresponding author. Tel.: 81-29-282-5461. Fax: 81-29-282-5663.
E-mail: iton@linac.tokai.jaeri.go.jp.

beams up to 8 MW, i.e. the energy is 1.5 GeV and the maximum average current is 5.3 mA.

A superconducting (SC) accelerator is the main option for the high energy part from 0.1 to 1.5 GeV because of its advantages; the length of the linac can be reduced without significant increase of the operating cost, the large bore radius is favorable for low beam loss, higher Q value is suitable for high duty and CW operation and inexpensive operating cost is expected in comparison with a normal conducting option. Up to now, various types of SC cavities have been widely used for electron and heavy ion accelerators, but there is no operated proton accelerator with SC cavities.

A design and development work of the SC linac has been continued since 1995 in collaboration with KEK. This paper describes the overview of the project and the present status of the conceptual design of the linac and cavity design work. The cavity development work is written in Ref. [2].

2. OVERVIEW OF THE NSP

Figure 1 shows the facility layout of the NSP. There are two main facilities; one is the neutron scattering facility and the other is the nuclear transmutation facility.

In the neutron scattering facility, basic investigations in the fields of material, biological and chemical science are made by the slow neutron scattering method. This facility requires intense short pulse beams to adopt the time-of-flight technique; i.e., the beam width is about 1 μs, the maximum repetition rate is 50 Hz and the maximum beam power is 5 MW. A storage ring compresses the beams to make the short pulse beams. The linac is required to produce negative hydrogen beams for injection to the ring and chopped beams for extraction from the ring.

In the nuclear transmutation facility, engineering studies are made for the accelerator driven nuclear waste transmutation system. For the engineering tests, this facility requires CW beams up to 8 MW. This requirement is one of the main reasons to choose the SC linac.

In addition, several facilities are proposed in the NSP; a nuclear physics facility, a spallation RI beam facility, a neutron

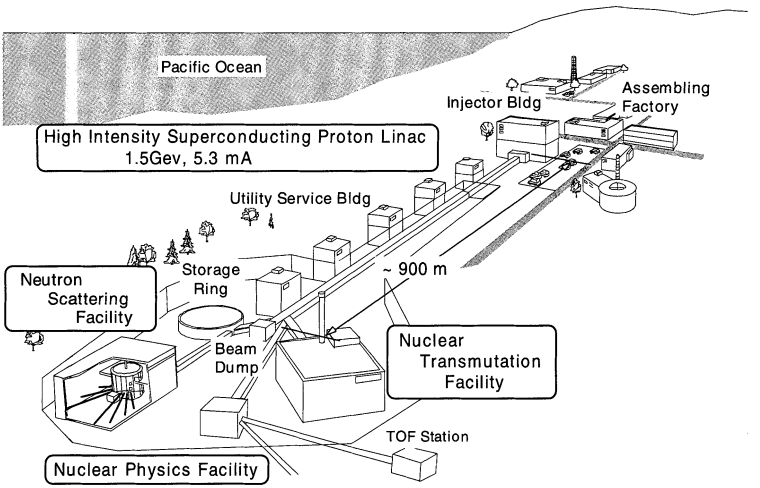

FIGURE 1 Facility layout of the Neutron Science Project (NSP).

irradiation facility and a meson/muon facility for the basic science investigations.[3]

The conceptual layout and specifications of the NSP linac are shown in Figure 2 and Table I, respectively. The linac accelerates both negative hydrogens and protons. Negative hydrogen beams are for the neutron scattering facility as described above and proton beams are for other facilities. Two stage commissioning has been proposed in the NSP; only pulse operation with the average current of 1 mA will be achieved in the first stage and both pulse and CW operation with the average current up to 5.3 mA will be made in the second stage. The injector below 0.1 GeV consists of an ion source, an RFQ and a DTL which are normal conducting (NC) devices. The high energy part from 0.1 to 1.5 GeV is an SC linac. The resonant frequencies of the NC cavities and SC cavities are 200 and 600 MHz, respectively.

Figure 3 shows the pulse structure of the linac beams for the neutron scattering facility. Macro-pulse width is 2–5.9 ms and the repetition rate is 50 Hz. Chopping provides intermediate-pulses in a macro-pulse; 400 ns for beam-on and 270 ns for beam-off. The peak current of the intermediate-pulses is 30 mA and the average current in a macro-pulses is 18 mA because of the 60% intermediate pulse duty.

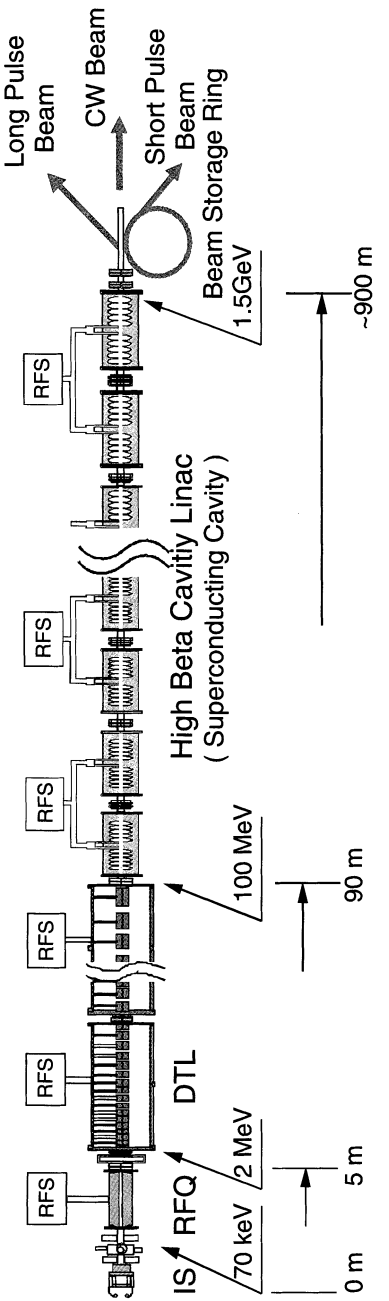

FIGURE 2 Conceptual layout of the NSP linac (IS: Ion Source, RFQ: Radio Frequency Quadrupole Linac, DTL: Drift Tube Linac).

TABLE I Specification of the NSP linac

Accelerating particle	H^-, H^+
Energy	1.5 GeV
Average current	1st stage 1 mA
	2nd stage 5.3 mA
Peak current	Nominal 30 mA
Low energy part	Normal conducting linac, Frequency 200 MHz
High energy part	Superconducting linac, Frequency 600 MHz
Beam operation	1st stage pulse
	2nd stage pulse/CW
Repetition rate	50 Hz
Macro-pulse width	2–5.9 ms, CW
Intermediate pulse width	400 ns (interval 270 ns)

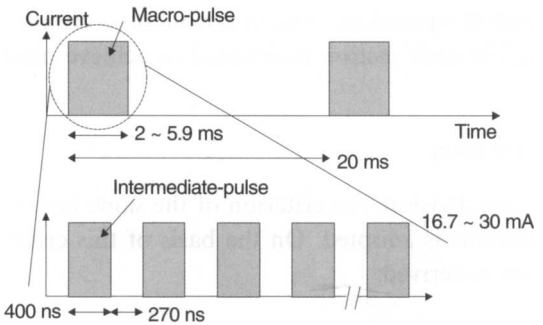

FIGURE 3 Pulse structure for the neutron scattering facility.

3. CONCEPTUAL DESIGN OF THE SC LINAC

In the SC linac for the NSP, β (ratio of particle velocity to light velocity) increases gradually from 0.43 to 0.92. Therefore, the SC cavities are to be divided into several sections with different β values to match to the proton velocity. In this section, the preliminary conceptual design is described including the section division, operating temperature and beam dynamics.

3.1. Basic Parameters for the Conceptual Design

Prior to the conceptual design of the NSP SC linac, basic parameters were prepared and are listed in Table II. Number of cells per cavity has

TABLE II Basic parameters for SC proton linac for the NSP

Cells/Cavity	5
Cavities/Module	2
Coupler/Cavity	1
Max. E_{peak}	16 MV/m
Focusing lattice	Doublet between modules
Synchronous phase	$-30°$

been determined to be 5 as results of considerations of the energy gain per cavity, the HOM effect, the coupler power and the effect of the microphonic vibration. As a guide line, the peak surface electric field (E_{peak}) is limited to be 16 MV/m with considerations of less refrigerator load and reliable operation. The criterion of constant accelerating gradient (E_{acc}) in each section is adopted to achieve uniform coupler power.

3.2. Section Division

To make section division, the criterion of the same behavior on phase slip for all sections is adopted. On the basis of this criterion, the following relation is derived:

$$\beta_1/\beta_0 = \beta_2/\beta_1 = \ldots = \beta_n/\beta_{n-1} = \beta_{c2}/\beta_{c1} = \beta_{c3}/\beta_{c2} = \ldots = \beta_{cn}/\beta_{cn-1},$$

where

n: number of sections,
β_0, β_n: β values for incident and output beam, respectively,
$\beta_1, \ldots, \beta_{n-1}$: β values at boundaries between adjacent sections,
$\beta_{c1}, \ldots, \beta_{cn}$: geometrical β values for the cavities in the sections.

As the result, the boundary β values ($\beta_1, \ldots, \beta_{n-1}$) are obtained by giving the number of sections. Subsequently, geometrical β values ($\beta_{c1}, \ldots, \beta_{cn}$) for the cavities are determined to minimize phase slip of protons in the cavities.

In general, larger number of sections can achieve higher accelerating efficiency, less number of cavities, shorter linac length and less emittance growth in the longitudinal phase space because of the less phase slip. For the capital and maintenance cost, the number of sections should not be increased so much. In order to optimize the number of

β sections, linac systems which consist of 4–8 sections have been considered. Our choice is 8-section scheme, which satisfies the length limitation in our site and is less expensive than the others on both capital and operating costs because of less number of cavities even considering to prepare the spare modules.

3.3. Parameters of Linac System

On the conceptual design work, a period of the beam line is assumed as shown in Figure 4. Space between the paired cavities in a module is 60 cm long and includes couplers. A distance between the cavity and quadrupole magnet is 70 cm. The conceptual design parameters are summarized in Table III. The total SC linac length is 733 m and the number of cavities is 308. The 7th and 8th sections exceed half of the linac system in length and in number of cavities. Lower β cavities up to $\beta = 0.6$ occupies only small parts of the total system. The E_{acc} value increase by β_c growth because the E_{peak} is set to be less than 16 MV/m and the ratio of E_{peak}/E_{acc} for low β_c are higher than that for high β_c. Coupler powers in Table III are found to be low enough for stable and reliable operation.

As an example of the phase behavior, Figure 5 represents the phase variation of the reference particles in the cells at the 2nd section. All of

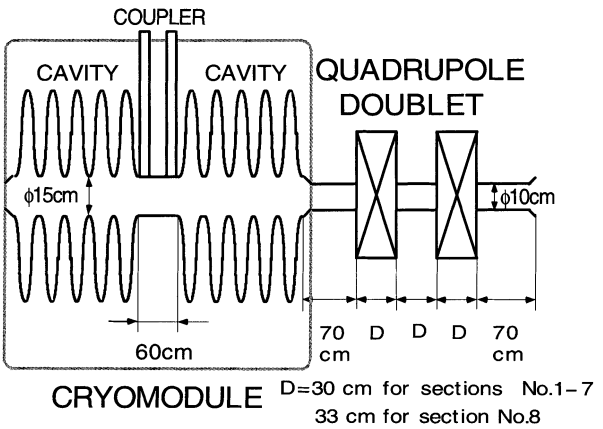

FIGURE 4 Schematic view of the beam line.

TABLE III Conceptual design parameters of the NSP SC proton linac

Section No.	1	2	3	4	5	6	7	8
Energy (MeV)	100–124	124–160	160–210	210–276	276–362	362–502	502–782	782–1504
β	0.428–0.468	0.468–0.520	0.520–0.576	0.576–0.635	0.635–0.692	0.692–0.759	0.759–0.838	0.838–0.923
β_c	0.453	0.499	0.549	0.604	0.665	0.732	0.805	0.886
No. of cavities	20	24	24	24	24	32	52	108
Length (m)	40.4	49.8	51.4	53.3	55.4	76.3	129.0	277.7
E_{acc} (MV/m)	2.45	2.86	3.56	4.30	5.01	5.59	6.23	7.03
Coupler power (kW)*	21	27	38	50	64	79	97	121

*Peak values for the pulse operation of 30 mA peak current and 60% intermediate pulse duty.

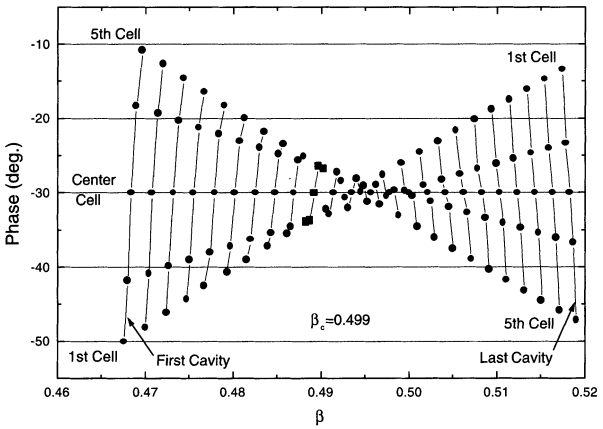

FIGURE 5 Phase variation of the reference particle in the cells for the 2nd section.

the phases in the center cell are $-30°$. Particles of $\beta < \beta_c$ are injected in the 1st cell at lower phase angle and exit from the 5th cell at higher phase angle. Particles of $\beta > \beta_c$ are injected at higher phase and exit at lower phase angle. Therefore, the maximum phase slips, $\pm 20°$, is seen in the end cells (1st and 5th cells) at the both end cavities of the section. The phase slip of the particles changes transit time factor of the cavity.[4] Figure 6 shows the transit time factor as a function of β value of the reference particles. In the design to minimize the phase slip, the transit time factor increases monotonically in each section because of an effect of leak fields to the beam tube as described in the next section. E_{peak} values, which are also plotted in Figure 6, vary to compensate the transit time factor degradation to keep E_{acc} constant in each section. Therefore, the maximum E_{peak} values, 16 MV/m, are found in the front end cavity in every section.

3.4. Operating Temperature

In order to determine the operating temperature, rough estimations of the refrigerator load have been made in the two cases of 2 K and 4 K systems on the basis of the KEK-TRISTAN experience. In the 2 K system, the cavity temperature is 2.0 K and the surface resistance is estimated to be 15 nΩ. Two kinds of thermal shields at 4–20 K and 80 K are considered in this system. In the 4 K system, the cavity temperature

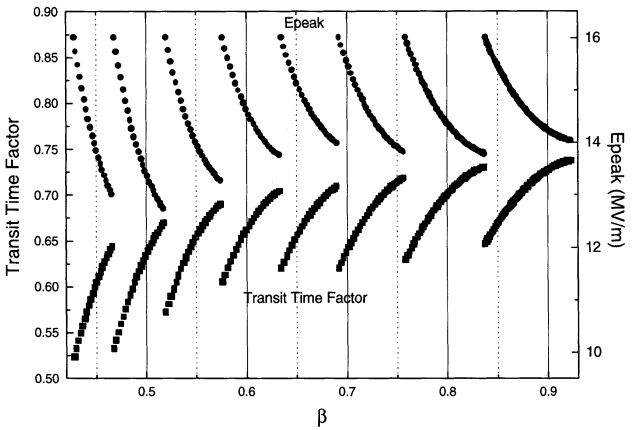

FIGURE 6 Transit time factor and E_{peak} as a function of the reference particle β.

TABLE IV Estimations of refrigerator load

	2 K *system*		4 K *system*
	2 K *load*	4–20 K *load*	4.4K *load*
RF load	2.6 kW		40 kW
Static loss			
Module	~0.5 kW	< 3 kW	~3 kW
Transfer line	~0.5	~3.6 kW	~3.6 kW
Total load	~3.6 kW	~6.6 kW	~46.6 kW
AC power	~3.6 MW	~2 MW	~14 MW

is 4.4 K and the surface resistance is 220 nΩ. Here, only one shield of 80 K is considered. The results are listed in Table IV, where refrigerator efficiencies are assumed to be 1/1000 and 1/300 for 2 K and 4.4 K loads, respectively. The heat load for 80 K shields are not listed in the table. The results indicate that the 2 K system has a greater advantage on the operating cost (AC power), as shown in the table, as well as on the capital cost. Therefore, the 2 K system is selected to be the main option for our design.

3.5. Lattice Design and Beam Dynamics

A lattice design has been carried out according to the placement of a doublet focusing magnet between modules as shown in Figure 4.

An equipartitioning scheme[5] is adopted in order to determine the focusing field strength. Lorentz stripping by magnetic fields has to be considered to avoid beam loss in the case of negative hydrogen acceleration. Therefore, the magnetic field is limited so that the loss rate due to the Lorentz stripping at $r = 5$ cm, which is a radius of the beam tube between the modules, should be less than 10^{-7}/m. Extended magnet length of 33 cm in 8th section (see Figure 4) is determined by this magnetic field limitation. The magnetic field gradients obtained in the lattice design work are in the range from 4.2 to 7.1 T/m.

The rms beam size and the normalized rms emittance calculated by the modified PARMILA code are plotted in Figures 7 and 8, respectively. The rms emittances of the incident beam, 0.08π cm·mrad and 0.865π deg.MeV for the transverse and longitudinal direction, respectively, have been estimated by the beam simulation of the injector up to 100 MeV. Because the maximum rms beam size is 0.33 cm, the ratio of the cavity bore radius (7.5 cm) to the rms beam size is more than 23. At the quadrupole doublet, the ratio of the beam tube radius (5 cm) to the rms beam size is more than 15. The rms emittances of the output beam have been evaluated to be 0.0827π cm·mrad and 0.889π deg.MeV for the transverse and longitudinal direction, respectively. Emittance growth on both transverse and longitudinal direction are very small because of the equipartitioning scheme.

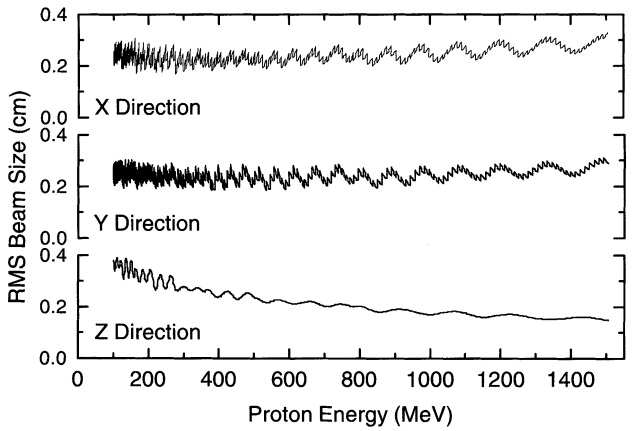

FIGURE 7 The rms beam size obtained by the beam simulation.

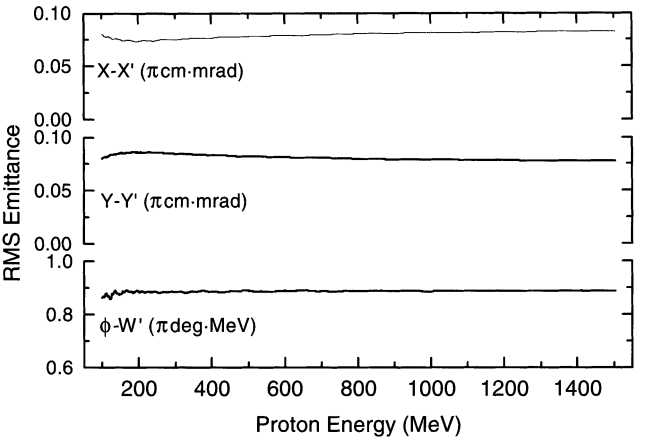

FIGURE 8 The normalized rms emittance obtained by the beam simulation.

4. CAVITY DESIGN WORK

As the first step of the cavity design, electromagnetic and structural analysis have been made on the half cell geometry and the preliminary design parameters were obtained.[6] The design work has been extended to the 5-cell cavity for all sections. Calculations of accelerating mode and HOM have been performed on the electromagnetic analysis. Structural analysis of the microphonic vibration and the deformation due to the Lorentz force have been carried out as well as the mechanical strength under the vacuum load.

4.1. Cavity Shape and Electromagnetic Analysis

The cavity shape parameters and the RF characteristics are summarized in Table V. The shape parameters are illustrated in Figure 9. Equator straight length for the end cell (L2′) is adjusted to achieve flat accelerating fields within 3%. The RF characteristics, R/Q, $E_{\text{peak}}/E_{\text{acc}}$ and $H_{\text{peak}}/E_{\text{acc}}$, depend on β; the values presented here were calculated at $\beta = \beta_c$.

A calculation in the 5-cell geometry with beam tube indicates the leak field to the beam tube. The leak field affects the accelerating voltage and the transit time factor of the cavity. In the case of a cavity in the 1st

TABLE V Cavity shape and RF characteristics

β_c	0.453	0.499	0.549	0.604	0.665	0.732	0.805	0.886
L (cm)	5.66	6.23	6.85	7.54	8.32	9.14	10.06	11.07
L' (cm)	5.44	6.00	6.61	7.29	8.07	8.88	9.82	10.84
b (cm)	22.80	22.69	22.59	22.51	22.42	22.37	22.30	22.25
R0 (cm)	2.45	2.86	3.31	3.83	4.44	5.03	5.82	6.68
R1 (cm)	1.58	1.75	1.92	2.10	2.30	2.60	2.82	3.10
R2 (cm)	3.17	3.50	3.84	4.20	4.60	5.20	5.63	6.20
α (deg.)	5.2	5.7	6.2	6.8	7.4	8.1	8.8	9.7
L2′ (cm)	0.28	0.27	0.25	0.25	0.25	0.26	0.26	0.27
R/Q* (Ω/cavity)	51.4	77.7	110.6	154.3	210.7	274.3	352.4	443.5
E_{peak}/E_{acc}*	5.56	4.65	3.92	3.40	2.95	2.57	2.25	2.04
H_{peak}/E_{acc}* (Oe/(MV/m))	113.2	94.5	81.5	71.3	63.0	57.1	51.2	47.4

*RF characteristics were calculated at $\beta=\beta_c$, $a=7.5$ cm for all cavities, L1 = 0.2 cm for all cavities, L2 = 0.5 cm for all cavities.

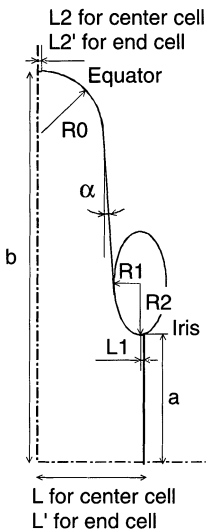

FIGURE 9 Cavity shape parameters.

section of $\beta_c = 0.453$, the energy gain is reduced by 9% by the leak field. This effect is small for high β_c cavities, i.e., 2% for $\beta_c = 0.886$ cavities. Figure 10 shows transit time factor as a function of β/β_c for a 5-cell $\beta_c = 0.453$ cavity with beam tube compared with that for the cavity which has no leak fields. The decrease of the transit time factor for the cavity with beam tube is due to the energy gain reduction by leak fields.

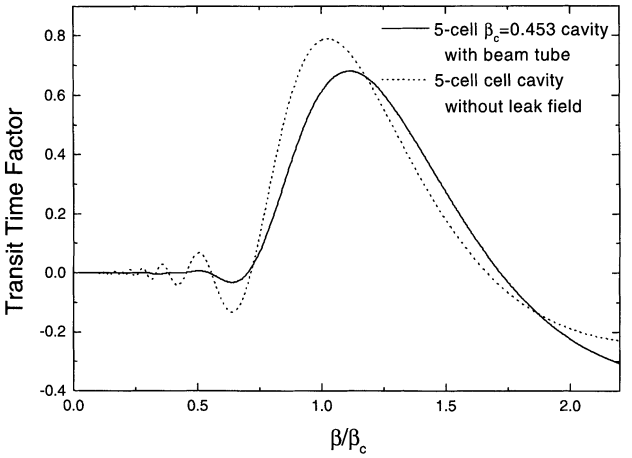

FIGURE 10 Transit time factor for 5-cell $\beta_c = 0.453$ cavity as a function of β/β_c.

The optimum β/β_c value goes up with the effect of leak fields, that is the reason of the monotonic increase of the transit time factor in each section as shown in Figure 6. In the conceptual design described in the previous section, additional one cell has been inserted in each beam tube to simulate leak fields on the calculation by the PARMILA code.

HOM analyses up to about 2 GHz have also been made to estimate R/Q, HOM voltage and power. We found that R/Q is very sensitive to the β value. For example, R/Q values of the TM020 modes for the 2nd section cavities of $\beta_c = 0.499$ are shown in Figure 11 as a function of β. R/Q's change over one order in the β range of the 2nd section. The HOM power per coupler has been estimated on the bases of the calculated R/Q values, the beam conditions and the coupling conditions of the HOM couplers. Two sets of beam tube HOM coupler were assumed for one cavity in this estimation. In the case of a $\beta_c = 0.499$ cavity, the estimated HOM power per coupler is less than 30 W, that is found to be low enough for stable and reliable operation.

4.2. Structural Analysis

For the first step of the structural analysis, cavity strength against static vacuum load has been estimated. The maximum von Mises' stresses

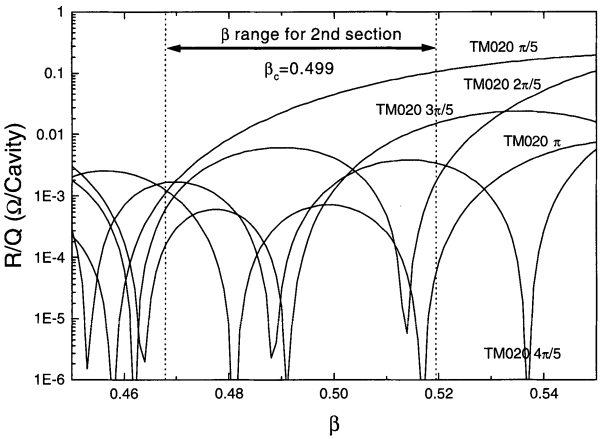

FIGURE 11 R/Q values of the TM020 modes as a function of β for the 2nd cavity.

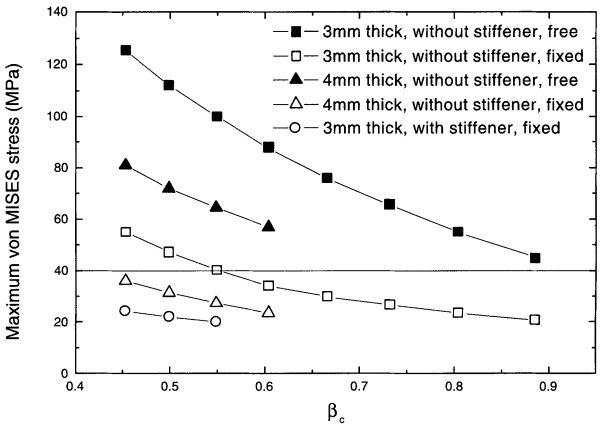

FIGURE 12 Maximum von Mises' stress of the cavity against static vacuum load.

for the vacuum load are represented in Figure 12. The calculation was carried out for several cases of 3 or 4 mm thick walls, without or with stiffener and the constraint conditions at the end of the cavity, fixed or free. To constrain both ends of the cavity is very effective in reducing von Mises' stress. The yield stress of niobium (RRR $\sim$ 200) at the room

temperature and corresponding allowable stress of the cavity are evaluated to be 60 and 40 MPa, respectively. Then, wall thickness of more than 4 mm or the stiffener is required for the cavities of $\beta_c < 0.6$. The choice will be made by considering the fabrication cost, microphonic vibration and the effects of Lorentz force.

For the pulse beam operation, the mechanical resonant frequencies are required to be higher than the maximum repetition rate of 50 Hz. Analysis for the mechanical resonance has been carried out to evaluate the microphonic vibration. Figure 13 shows an example of the vibration which is the lowest frequency mode, axial mode of 80 Hz, for the $\beta_c = 0.499$ cavity of 3 mm thick wall with stiffener. We found that the stiffener is effective to increase the structural resonant frequency; in the case without stiffener, the lowest mode is in transverse direction and the frequency is 38 Hz.

Estimation of the cavity detuning due to the Lorentz force, which is also important for the pulse operation, has been carried out by combining structural and electromagnetic analysis. Figure 14 shows the frequency shift by the Lorentz force with comparison of the cavity band widths which are derived from the coupler powers. The analysis was made for the niobium cavities of 3 mm wall thickness with and without stiffener. In the case without stiffener, the frequency shifts for the cavities of $\beta_c < 0.5$ are comparable to their band width. The stiffeners are effective to reduce the frequency shifts as shown in Figure 14. The contact positions of the stiffener are optimized for the vacuum load

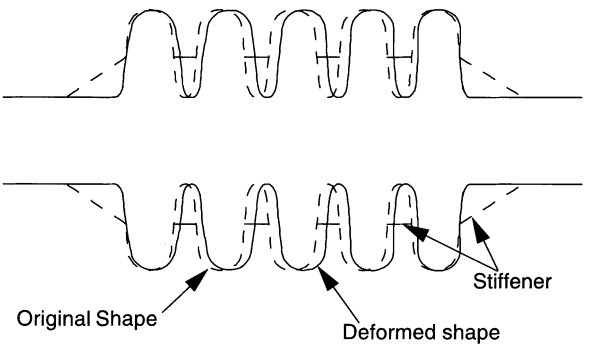

FIGURE 13 Lowest vibration mode (80Hz) for the $\beta_c = 0.499$ cavity of 3 mm thick wall with stiffener.

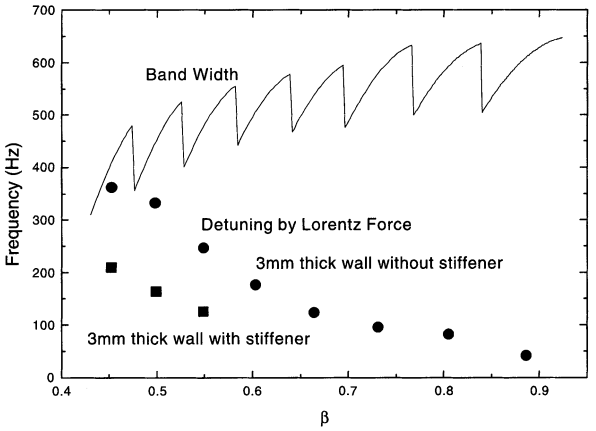

FIGURE 14 Frequency shift by Lorentz force (given in absolute values) and the cavity band width.

but not for the Lorentz force. Thus, additional reduction of frequency shift is expected by optimizing the stiffener contact position for the Lorentz force. This analysis was performed for the CW excitation. The estimations of response for the pulse excitation are being performed.

5. CONCLUSION

Design and development work on the high intensity superconducting proton linac for the NSP has been proceeding in JAERI. The preliminary conceptual design, including linac system, operating temperature, lattice design and beam dynamics, was discussed. The cavity design for electromagnetic and structural characteristics was carried out. In the cavity development work for the $\beta_c = 0.5$ single-cell cavity,[2] the Q value of about 2×10^{10} in the low field measurement and the maximum E_{peak} value of 30 MV/m have been achieved at the temperature of 2 K.

Further optimization of the design is currently continued. The first reference of the SC linac design including the cryomodule and the refrigerator will be made in the next year.

References

[1] M. Mizumoto *et al.*, *Proc. of the 18th Int. Linear Accelerator Conf.*, Geneva, Switzerland, p. 662 (1996).
[2] N. Ouchi *et al.*, Design and development work for a superconducting proton linac at JAERI, *Proc. of the 8th Workshop on RF Superconductivity*, Abano Terme (Padova), Italy (1997).
[3] T. Mukaiyama *et al.*, *Proc. of Topical Meeting on Nuclear Applications of Accelerator Technology*, Albuquerque, USA, p. 398 (1997).
[4] R.W. Garnett and T.P. Wangler, *Proc. of the 18th Int. Linear Accelerator Conf.*, Geneva, Switzerland, p. 707 (1996).
[5] M. Reiser, *Theory and Design of Charged Particle Beams*, John Wiley & Sons, Inc. (1994).
[6] N. Ito *et al.*, *Proc. of the 18th Int. Linear Accelerator Conf.*, Geneva, Switzerland, p. 671 (1996).